Frontiers in Bioscience Landmark

Front. Biosci. (Landmark Ed) **2026**; 31(7): 50499
https://doi.org/10.31083/FBL50499

Original Research

Ifi27l2a is a Candidate Gene Associated With Osteoclast-Related Transcriptional Remodeling in the Aging Bone Marrow

Yuqi Li[1], Wenbin Zhou[1], Yuancan Xiao[1], Jideng Ma[2], Lixin Wei[1,*], Lei Jiang[1,*]

[1]Qinghai Provincial Key Laboratory of Tibetan Medicine Pharmacology and Safety Evaluation, Northwest Institute of Plateau Biology, Chinese Academy of Science, 810001 Xining, Qinghai, China
[2]Clinical Medical College, Qinghai University, 810001 Xining, Qinghai, China
*Correspondence: lxwei@nwipb.cas.cn (Lixin Wei); jianglei@nwipb.cas.cn (Lei Jiang)
Academic Editor: Elisa Belluzzi
Submitted: 29 January 2026 Revised: 30 April 2026 Accepted: 21 May 2026 Published: 17 July 2026

Abstract

Introduction: Age-related bone loss is closely linked to inflammaging in the bone marrow microenvironment, but the molecular factors connecting immune remodeling to bone metabolic imbalance remain incompletely defined. This study aimed to identify aging-associated genes related to inflammatory remodeling in the bone marrow and to provide preliminary cellular evidence for a prioritized candidate. **Methods:** Public bulk RNA-seq (GSE132040) and single-cell RNA-seq (GSE132042) datasets from physiologically aging mice were analyzed using an integrated workflow. Differentially expressed genes (DEGs) were identified from bulk RNA-seq data, followed by Gene Ontology (GO) and Gene Set Enrichment Analysis (GSEA). Candidate genes were prioritized using least absolute shrinkage and selection operator (LASSO) regression and support vector machine-recursive feature elimination (SVM-RFE). Single-cell RNA-seq was used to examine the cellular distribution of the candidate gene within bone marrow cell populations. For cellular validation, *Ifi27l2a* was knocked down in RAW264.7 cells using lentiviral shRNA, followed by quantitative reverse transcription polymerase chain reaction (RT-qPCR) and transcriptomic analysis. Primary bone marrow-derived macrophages (BMMs) were further used for TRAP staining-based assessment under M-CSF/RANKL-induced osteoclastogenic conditions. **Results:** A total of 313 DEGs were identified between young and aged bone marrow samples, with enrichment mainly in antiviral, host-defense, and immune-related processes. Integrated LASSO and SVM-RFE screening prioritized *Ifi27l2a* for further analysis. Whole-bone-marrow bulk RNA-seq analysis showed an age-associated decline in *Ifi27l2a* expression, whereas single-cell analysis showed a monocyte-enriched distribution. In RAW264.7 cells, *Ifi27l2a* knockdown reduced *Il6* and *Tnf* expression and was accompanied by broader transcriptomic remodeling involving inflammatory programs and osteoclast-related transcriptional changes. Pathway analysis showed significant positive enrichment of the rheumatoid arthritis pathway and suggestive enrichment of the osteoclast differentiation pathway. In primary BMMs, TRAP staining showed that *Ifi27l2a* knockdown was associated with altered osteoclast-like morphology under M-CSF/RANKL stimulation. **Conclusion:** These findings identify *Ifi27l2a* as a bone marrow aging-associated candidate gene with monocyte-enriched expression and a potential link to inflammatory and osteoclast-lineage remodeling. The current study supports an association between *Ifi27l2a* reduction, macrophage-lineage transcriptional remodeling, and osteoclast-like morphological changes, rather than definitive causality. Further *in vivo* validation of bone phenotypes and pathway-level studies are needed to clarify its role in age-related bone remodeling.

Keywords: bone marrow; aging; macrophages; osteoclasts; inflammation; RNA-Seq

1. Introduction

Aging is a systemic process accompanied by progressive changes in both immune function and skeletal homeostasis. Under physiological conditions, bone marrow immunity and bone remodeling are closely coordinated; however, this balance becomes increasingly disturbed with age, contributing to an imbalance in bone metabolism and osteoporosis in older individuals [1,2]. Because the bone marrow niche contains multiple interacting immune, hematopoietic, and stromal cell populations, and because immune mediators exert broad effects on both hematopoiesis and bone remodeling, the molecular links between inflammaging and age-related bone loss remain incompletely understood [2].

As a central hematopoietic and immune organ, bone marrow undergoes substantial microenvironmental remodeling during aging and gradually develops features of chronic low-grade inflammation [3,4]. Age-related alterations in the bone marrow niche can impair hematopoietic stem cell support, promote myeloid skewing, and disturb local immune homeostasis [3,4]. Among the cellular components involved, monocytes and macrophages are increasingly recognized not only as responders to inflammatory stress but also as contributors to inflammatory remodeling in aged tissues [5,6]. In the aging bone marrow microenvironment, these cells may undergo phenotypic and functional alterations and participate in the production of inflammatory mediators, including tumor necrosis factor-α (TNF-α), interleukin-1β (IL-1β), and interleukin-6 (IL-6), thereby aggravating local inflammatory stress and disrupting microenvironmental homeostasis [1,2,5].

The inflammatory bone marrow microenvironment has important consequences for skeletal metabolic homeostasis. Immune activation and increased production of pro-osteoclastogenic mediators, including receptor activator of nuclear factor-κB ligand (RANKL), TNF-α, IL-1β, IL-6, IL-17, and macrophage colony-stimulating factor (M-CSF), can promote osteoclast differentiation and bone resorption, ultimately disturbing the balance of bone remodeling [7,8]. This osteoimmune dysregulation is particularly evident in chronic inflammatory diseases such as rheumatoid arthritis (RA), in which persistent cytokine activation contributes to focal bone erosion and systemic bone loss [9]. Consistently, improved control of inflammation and the use of biologic therapies have been associated with attenuation of inflammation-related bone loss and improved bone outcomes in RA [9,10].

Among genes potentially involved in immune remodeling within aged bone marrow, *Ifi27l2a* emerged from our screening workflow as a candidate of interest. *Ifi27l2a* is an interferon-stimulated gene, but its role in the aging bone marrow microenvironment and its relationship with osteoclast-lineage remodeling remain poorly defined.

In the present study, we analyzed two publicly available transcriptomic datasets from naturally aged mice in the Gene Expression Omnibus (GEO) database to identify genes associated with inflammatory remodeling during bone marrow aging. Differentially expressed genes were characterized by Gene Ontology (GO) analysis and Gene Set Enrichment Analysis (GSEA), and candidate genes were prioritized using least absolute shrinkage and selection operator (LASSO) regression and support vector machine-recursive feature elimination (SVM-RFE). This integrative analysis identified *Ifi27l2a* as a bone marrow aging-associated candidate gene. Subsequent cellular experiments using RAW264.7 cells and primary bone marrow-derived macrophages further supported an association between *Ifi27l2a* knockdown, macrophage-lineage transcriptional remodeling, and altered osteoclast-like differentiation.

2. Materials and Methods

2.1 Data Collection and Download

Publicly available transcriptomic datasets were obtained from the Gene Expression Omnibus (GEO) database. Bulk RNA-seq data from mouse bone marrow samples collected across the lifespan were obtained from GEO under accession number GSE132040 [11]. To further examine the cellular distribution of genes of interest within the heterogeneous bone marrow compartment, publicly available single-cell RNA-seq data were obtained from GEO under accession number GSE132042 [12].

2.2 Bioinformatic Analysis of Aging Datasets

For bulk RNA-seq analysis, samples from 6–9 months of age were defined as the young group, whereas samples from 21–27 months of age were defined as the old group, consistent with a previously reported analytic strategy for this dataset [13]. Raw count matrices were analyzed using R software (version 4.3.0; R Foundation for Statistical Computing, Vienna, Austria; https://www.R-project.org/) with the DESeq2 package (version 1.40.2; Bioconductor Project; https://bioconductor.org/packages/DESeq2/) [14]. Differentially expressed genes (DEGs) were identified using the thresholds of $|\log2FoldChange| \geq 0.3$ and adjusted $p < 0.05$. Functional annotation was performed using the clusterProfiler package (version 4.8.1; Bioconductor Project; https://bioconductor.org/packages/clusterProfiler/), including Gene Ontology (GO) enrichment analysis and Gene Set Enrichment Analysis (GSEA) [15].

2.3 Feature Selection by Least Absolute Shrinkage and Selection Operator and Support Vector Machine-Recursive Feature Elimination

To prioritize genes associated with transcriptional aging in bone marrow, two feature-selection methods were applied to the age-associated expression matrix. Chronological age was used as the continuous response variable in both feature-selection analyses. Least absolute shrinkage and selection operator (LASSO) regression was implemented using the glmnet package [16], and support vector machine-recursive feature elimination (SVM-RFE) was performed using the caret framework [17]. For LASSO, 10-fold cross-validation was used to determine the optimal penalty parameter λ based on the mean squared error, and genes with non-zero coefficients at lambda. min were retained. For SVM-RFE, hyperparameters were optimized by grid search with 10-fold cross-validation, and the feature subset with the minimum cross-validated root mean squared error was retained. The overlap between LASSO- and SVM-RFE-derived candidates was used for downstream prioritization.

2.4 Single-Cell RNA-seq Data Processing and Analysis

Single-cell RNA-seq analysis and visualization were performed using Scanpy software (version 1.9.1; scverse project, open-source Python package; https://scanpy.readthedocs.io/) [18]. Quality control (QC) was implemented by filtering out cells with a mitochondrial gene fraction > 20%. Raw counts were normalized to 10,000 counts per cell, log-transformed, and batch-corrected using BBKNN software (version 1.6.0; Teich Lab, open-source Python package; https://github.com/Teichlab/bbknn) [19]. Cell populations were visualized using Uniform Manifold Approximation and Projection (UMAP), and candidate-gene expression patterns were evaluated across annotated bone marrow cell compartments. Cell-type annotations from the original dataset were used for downstream visualization and candidate-gene localization. No additional monocyte subcluster annotation, trajectory inference, or cell–cell communication analysis was performed in the present study.

2.5 Cell Culture

RAW264.7 murine macrophages were obtained from Procell Life Science & Technology Co., Ltd. (Wuhan, China), which originally sourced the cell line from ATCC (Manassas, VA, USA). According to the supplier's quality-control certificates, the RAW264.7 cell line was authenticated by mouse short tandem repeat (STR) profiling and tested negative for mycoplasma contamination using a PCR-based mycoplasma detection assay before use.

RAW264.7 cells were maintained in high-glucose DMEM (Gibco, Thermo Fisher Scientific, Waltham, MA, USA) supplemented with 10% fetal bovine serum (FBS, Gibco) and 1% penicillin-streptomycin. Cells were cultured at 37 °C in a humidified incubator with 5% CO_2 and passaged every 2–3 days. Only low-passage cells were used for downstream experiments. In this study, RAW264.7 cells were used for lentiviral knockdown, inflammatory gene-expression analysis, and transcriptomic sequencing, whereas primary BMMs were used to examine TRAP-positive osteoclast-like morphological changes under M-CSF/RANKL-induced osteoclastogenic conditions.

2.6 Lentivirus-Mediated *Ifi27l2a* Knockdown in RAW264.7 Cells

Stable *Ifi27l2a*-knockdown RAW264.7 cell pools were established using a pLKO.1-puro/RFP lentiviral system. Lentiviral particles encoding either an *Ifi27l2a*-targeting shRNA (SH3 group) or a non-targeting control shRNA (SHB group; sequence: 5′-CAACAAGATGAAGAGCACCAA-3′) were custom-generated by Anhui General Biological Systems Co., Ltd. using HEK293T-based packaging with psPAX2 and pMD2.G helper plasmids. Viral stocks were supplied at a titer of 1×10^8 TU/mL and stored at −80 °C until use.

For transduction, RAW264.7 cells were seeded into 6-well plates at 5×10^4 cells per well and allowed to adhere overnight. Cells were then incubated with lentiviral particles at a multiplicity of infection (MOI) of 10 in complete medium containing 5 μg/mL polybrene (Sigma-Aldrich, St. Louis, MO, USA). After 24 h, the viral supernatant was replaced with fresh complete medium. Transduction efficiency was assessed 72 h later by RFP fluorescence. To establish stable polyclonal pools, transduced cells were selected with puromycin at 2 μg/mL for 7–10 days. In the present study, the term "stable knockdown cell pools" refers to puromycin-selected, RFP-positive polyclonal RAW264.7 populations in which reduced *Ifi27l2a* expression was subsequently confirmed by RT-qPCR and transcriptomic analysis.

2.7 Validation of Ifi27l2a Knockdown Efficiency

Total RNA was extracted using TRIzol reagent (Invitrogen, Carlsbad, CA, USA; cat. no. 15596026). RNA concentration and purity were assessed using a NanoDrop 2000 spectrophotometer (Thermo Fisher Scientific, Wilmington, DE, USA). cDNA was synthesized from 1 μg of total RNA using the PrimeScript RT reagent kit with gDNA Eraser (Perfect Real Time; Takara Bio Inc., Kusatsu, Shiga, Japan; cat. no. RR047A). Quantitative PCR was performed on a StepOnePlus Real-Time PCR System (Applied Biosystems, Foster City, CA, USA) using SYBR Premix Ex Taq II (Tli RNaseH Plus; Takara Bio Inc., Kusatsu, Shiga, Japan; cat. no. RR820A). The thermal cycling conditions were 95 °C for 30 s, followed by 40 cycles of 95 °C for 5 s and 60 °C for 30 s. Melting-curve analysis was performed from 65 °C to 95 °C to confirm primer specificity. Relative expression was normalized to Gapdh and calculated using the $2^{-\Delta\Delta Ct}$ method. Knockdown efficiency was confirmed before downstream RNA-seq and osteoclast-related assays.

The primer sequences were as follows: *Ifi27l2a* forward, 5′-ACTGTTTGGCTCTGCCATAGG-3′; *Ifi27l2a* reverse, 5′-GCCTGCTGATTGGAGTGTGG-3′; Gapdh forward, 5′-TTCACCACCATGGAGAAGGC-3′; and Gapdh reverse, 5′-GGCATGGACTGTGGTCATGA-3′.

2.8 Primary BMM Isolation, Lentiviral Knockdown, Osteoclast Induction, and TRAP Staining

Primary bone marrow-derived macrophages (BMMs) were prepared from male C57BL/6 mice aged 6–8 weeks to assess osteoclast-like morphological responses to *Ifi27l2a* knockdown in a primary macrophage-lineage system. Three mice were used for independent BMM isolation, and each independent BMM preparation was considered a biological replicate. Because the mice were used solely as donors for primary BMM isolation and were not assigned to any in vivo intervention or treatment groups, animal-level randomization was not applicable. For downstream cell-based experiments, BMMs from each independent donor preparation were allocated to the indicated treatment groups at the culture-well level and processed in parallel under the same predefined experimental workflow to minimize potential procedural confounding. Mice were deeply anesthetized with 4% isoflurane in oxygen in an induction chamber until loss of the pedal withdrawal reflex and then euthanized by cervical dislocation before femur collection. Bone marrow cells were flushed from the femurs under sterile conditions and cultured for BMM preparation. The cells were subsequently subjected to lentiviral knockdown, M-CSF/RANKL-induced osteoclastogenic induction, and TRAP staining-based assessment. The protocol involving the isolation of primary BMMs from C57BL/6 mice was approved by the Committee of the Northwest Institute of Plateau Biology, Chinese Academy of Sciences (License No. NWIPB2025–46), and all animal-related procedures were conducted in accordance with the ARRIVE guidelines and institutional guidelines for the care and use of laboratory animals.

Bone marrow cells were flushed from the femurs under sterile conditions and cultured in α-MEM supplemented with 10% FBS, 1% penicillin-streptomycin, and recom-

binant mouse macrophage colony-stimulating factor (M-CSF, 30 ng/mL) to enrich macrophage-lineage cells. Non-adherent cells were removed during medium replacement, and adherent macrophage-lineage cells were further maintained in M-CSF-containing medium before subsequent experiments.

Following the RAW264.7 knockdown strategy, primary BMMs were divided into WT, SHB, and SH3 groups. WT cells were left untreated, SHB cells were transduced with the non-targeting shRNA lentivirus, and SH3 cells were transduced with the *Ifi27l2a*-targeting shRNA lentivirus. Lentiviral transduction was performed using the lentiviral constructs described above in the presence of polybrene at 5 μg/mL. After transduction, cells were maintained in M-CSF-containing medium, and knockdown efficiency was confirmed before osteoclast differentiation.

For osteoclast differentiation, WT, SHB, and SH3 BMMs were cultured in α-MEM containing 10% FBS, M-CSF at 30 ng/mL, and recombinant mouse RANKL at 50 ng/mL. The induction medium was replaced every 2 days. At the end of the induction period, cells were fixed and stained for tartrate-resistant acid phosphatase (TRAP) using a commercial TRAP staining kit according to the manufacturer's instructions. TRAP staining was performed to examine osteoclast-like morphological changes after *Ifi27l2a* knockdown in primary macrophage-lineage cells under M-CSF/RANKL-induced osteoclastogenic conditions.

2.9 Transcriptomic Sequencing and Analysis of Knockdown Cells

Total RNA from three biological replicates of SHB and SH3 stable RAW264.7 cell pools was submitted for library construction and sequencing on the Illumina NovaSeq 6000 platform (Illumina, San Diego, CA, USA) by BGI (Shenzhen, Guangdong, China). Raw sequencing quality was evaluated using FastQC software (version 0.11.9; Babraham Bioinformatics; https://www.bioinformatics.babraham.ac.uk/projects/fastqc/), and adapter trimming and low-quality read filtering were performed using Trimmomatic software (version 0.39; Usadel Lab; http://www.usadellab.org/cms/?page=trimmomatic). Clean reads were aligned to the mouse reference genome (GRCm39) using HISAT2 software (version 2.2.1; Daehwan Kim Lab/Center for Computational Biology, Johns Hopkins University, Baltimore, MD, USA; https://daehwankimlab.github.io/hisat2/). Transcript assembly and gene-level quantification were performed using StringTie software (version 2.2.1; Center for Computational Biology, Johns Hopkins University, Baltimore, MD, USA; https://ccb.jhu.edu/software/stringtie/), and count matrices were used for differential expression analysis in DESeq2 package (version 1.38.3; Bioconductor Project; https://bioconductor.org/packages/DESeq2/).

For this validation dataset, DEGs were defined using the thresholds of |log2FoldChange| >1 and adjusted $p < 0.05$. FPKM values were used only for visualization. Functional enrichment analysis, including GO, Kyoto Encyclopedia of Genes and Genomes (KEGG), and GSEA, was performed using clusterProfiler package (version 4.2.2; Bioconductor Project; https://bioconductor.org/packages/clusterProfiler/). For GSEA, genes were ranked according to differential-expression statistics, and pathway-level results were interpreted with caution when the adjusted significance was borderline.

2.10 Statistical Analysis

All statistical analyses were performed using R software (version 4.3.0; R Foundation for Statistical Computing, Vienna, Austria; https://www.R-project.org/) and GraphPad Prism (version 9.0; GraphPad Software, LLC, Boston, MA, USA; https://www.graphpad.com/). Cell-based quantitative experiments were performed with at least three independent biological replicates unless otherwise stated. Data are presented as mean ± standard deviation (SD). For non-omics cell-based quantitative comparisons between two groups, an unpaired two-tailed Student's *t*-test was used. For quantitative comparisons involving three groups, namely WT, SHB, and SH3, one-way analysis of variance (ANOVA) followed by Tukey's post hoc test was applied. A two-sided p value < 0.05 was considered statistically significant. All graphs were generated using ggplot2 package (version 3.4.2; tidyverse team; https://ggplot2.tidyverse.org/) or GraphPad Prism, and the statistical details for each quantitative analysis are provided in the corresponding figure legends.

3. Results

3.1 Age-Associated Transcriptional Alterations and Functional Enrichment in Mouse Bone Marrow

Bulk RNA-seq data from GSE132040 were analyzed to define age-associated transcriptional alterations in mouse bone marrow. Samples from mice aged 6–9 months were assigned to the young cohort, whereas those from mice aged 21–27 months were assigned to the aged cohort. Using predefined thresholds of |log2FoldChange| ≥0.3 and adjusted $p < 0.05$, we identified 313 differentially expressed genes (DEGs) between aged and young bone marrow samples, comprising 264 upregulated and 49 downregulated genes in the aged group.

The heatmap revealed distinct age-related expression patterns among these DEGs across the examined age groups, suggesting gradual remodeling of the bone marrow transcriptomic landscape during aging (Fig. 1A). The volcano plot displayed the overall distribution of DEGs between the aged and young cohorts and marked several representative age-associated genes, including *Ifi27l2a*, *Oas2*, *Tnf*, *Bcl2a1b*, *Egr1*, and *Cxcl5* (Fig. 1B).

GO enrichment analysis was then performed to investigate the biological processes represented by these age-related DEGs. The enrichment map showed that the en-

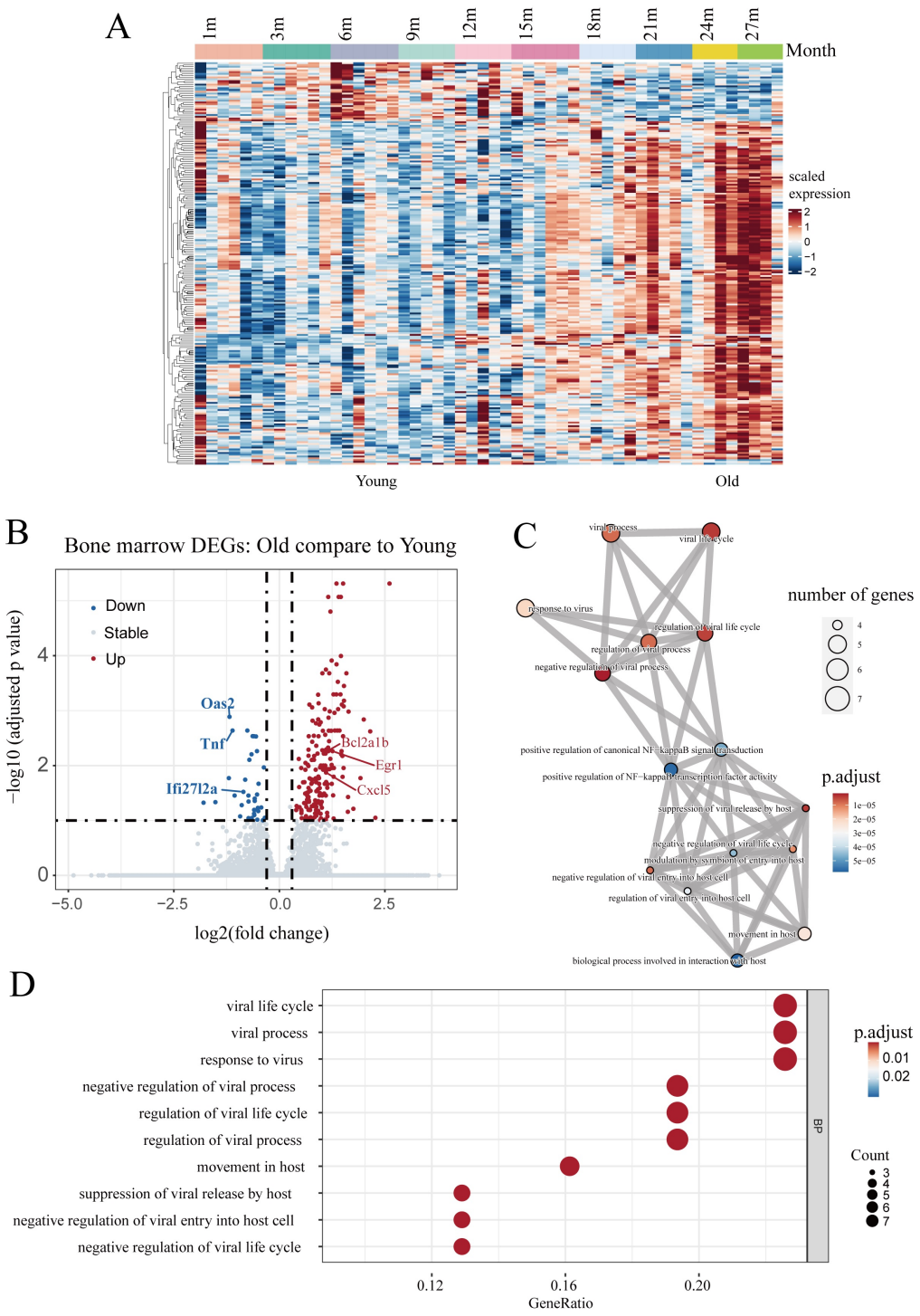

Fig. 1. Age-associated transcriptional alterations and GO enrichment analysis in mouse bone marrow. (A) Heatmap showing the expression patterns of 313 DEGs across the examined age groups. Among these DEGs, 264 genes were upregulated and 49 genes were downregulated in aged bone marrow samples compared with young samples. (B) Volcano plot showing differentially expressed genes (DEGs) between the young cohort, defined as mice aged 6–9 months, and the aged cohort, defined as mice aged 21–27 months. DEGs were identified using thresholds of |log2FoldChange| ≥0.3 and adjusted $p < 0.05$. (C) Enrichment map showing the connectivity among significantly enriched Gene Ontology (GO) Biological Process terms. Nodes represent enriched terms, node size indicates the number of associated DEGs, and node color represents the adjusted p value. Edges indicate shared genes between terms. (D) Dot plot showing the top enriched GO Biological Process terms. The enriched terms were primarily related to antiviral and host-defense responses, including viral life cycle, viral process, response to virus, negative regulation of viral process, and regulation of viral life cycle.

riched terms were highly interconnected and were mainly related to antiviral and host-defense responses, including viral life cycle, viral process, response to virus, and regulation of viral process (Fig. 1C). Similarly, the GO Biological Process dot plot showed prominent enrichment of defense-associated terms, such as viral life cycle, viral process, response to virus, negative regulation of viral process, and regulation of viral life cycle (Fig. 1D). These results indicate that bone marrow aging is accompanied by substantial remodeling of immune- and virus-response-related transcriptional programs.

GSEA was further applied to examine pathway-level trends across the aging-associated expression profile. In line with the GO enrichment results, several immune-related signatures, including immune effector process, production of molecular mediator of immune response, humoral immune response, and hemostasis, showed enrichment in the aging-related expression pattern (**Supplementary Fig. 1A–D**). Together, these analyses suggest that aging reshapes the bone marrow transcriptome toward immune-associated remodeling, with notable involvement of antiviral and host-defense-related biological processes.

3.2 Feature-Selection Analysis Prioritizes Ifi27l2a *as a Candidate Gene Associated With Bone Marrow Aging*

LASSO regression and SVM-RFE were applied to the DEG matrix from the bulk RNA-seq dataset to refine the list of age-associated genes. The LASSO model, using 10-fold cross-validation, retained 10 genes with nonzero coefficients at the optimal lambda value (Fig. 2A). SVM-RFE selected 37 genes at the point of minimum cross-validation RMSE, representing the feature subset with the best cross-validated performance for predicting chronological age (Fig. 2B).

The intersection of the two feature-selection approaches yielded six shared candidate genes: *Ifi27l2a*, *Oas2*, *Egr1*, *Cxcl5*, *Tnf*, and *Bcl2a1b* (Fig. 2C). Their expression patterns were then examined in the bulk RNA-seq dataset. Among these candidates, *Ifi27l2a* and *Oas2* showed relatively clear age-associated expression differences, with *Ifi27l2a* displaying a consistent decrease in aged bone marrow samples (Fig. 2D and **Supplementary Fig. 2A–E**). Given its reproducible decline during aging and its selection by both feature-selection methods, *Ifi27l2a* was prioritized for subsequent analysis.

The cellular distribution of the candidate genes was further examined using the single-cell RNA-seq dataset GSE132042. The dot plot showed heterogeneous expression patterns across annotated bone marrow cell populations, with *Ifi27l2a* showing relatively enriched expression in monocyte-lineage cells (Fig. 2E). UMAP visualization resolved the major hematopoietic and immune cell populations in mouse bone marrow and further highlighted the monocyte-related compartment within the bone marrow landscape (Fig. 2F and **Supplementary Fig. 3**). Together, these results nominated *Ifi27l2a* as an aging-associated candidate gene with bulk-level expression changes and monocyte-enriched expression in the bone marrow microenvironment.

3.3 Single-Cell Analysis Reveals Monocyte-Enriched Ifi27l2a Expression During Bone Marrow Aging

To define the cellular context of *Ifi27l2a* expression during bone marrow aging, we compared its expression pattern in total bone marrow cells and in the annotated monocyte subset using the single-cell RNA-seq dataset. In total bone marrow cells, *Ifi27l2a* showed a decreasing trend at later ages, consistent with its reduced expression in aged samples in the bulk RNA-seq analysis (Fig. 3A). When the analysis was restricted to bone marrow monocytes, however, *Ifi27l2a* remained prominently expressed across the examined age groups (Fig. 3B).

UMAP visualization further localized *Ifi27l2a* expression to the annotated monocyte population (Fig. 3C). Quantification of mean *Ifi27l2a* expression within monocytes showed no significant age-dependent difference, indicating that its expression was relatively maintained within this cell population (Fig. 3D). A direct comparison of expression trends between total bone marrow cells and monocytes showed that the decline in *Ifi27l2a* expression was more evident at the whole-bone-marrow level than within the monocyte subset (Fig. 3E). These findings suggest that monocytes constitute a major *Ifi27l2a*-expressing compartment in the bone marrow, and that the reduced *Ifi27l2a* signal observed in bulk bone marrow may partly reflect age-related changes in cellular composition rather than a uniform decrease within monocytes.

3.4 Ifi27l2a Knockdown is Associated With Inflammatory Gene Changes, Transcriptomic Remodeling, and Altered Osteoclast-Like Differentiation

To examine the potential involvement of *Ifi27l2a* in macrophage-lineage cells, a lentiviral shRNA-mediated knockdown model was established. WT cells served as untreated controls, SHB cells were transduced with a non-targeting shRNA, and SH3 cells were transduced with an *Ifi27l2a*-targeting shRNA. RFP fluorescence was detected in SHB and SH3 cells but was absent in WT cells, confirming successful lentiviral transduction (Fig. 4A). RT-qPCR analysis showed a marked reduction in *Ifi27l2a* mRNA expression in SH3 cells compared with SHB cells, and this decrease was further supported by RNA-seq-derived normalized read counts (Fig. 4C,F).

Primary BMMs were further used to examine osteoclast-like morphological changes under M-CSF/RANKL-induced osteoclastogenic conditions. TRAP staining showed TRAP-positive osteoclast-like cells with multinucleated features in the WT and SHB groups, whereas SH3 cells displayed a less prominent

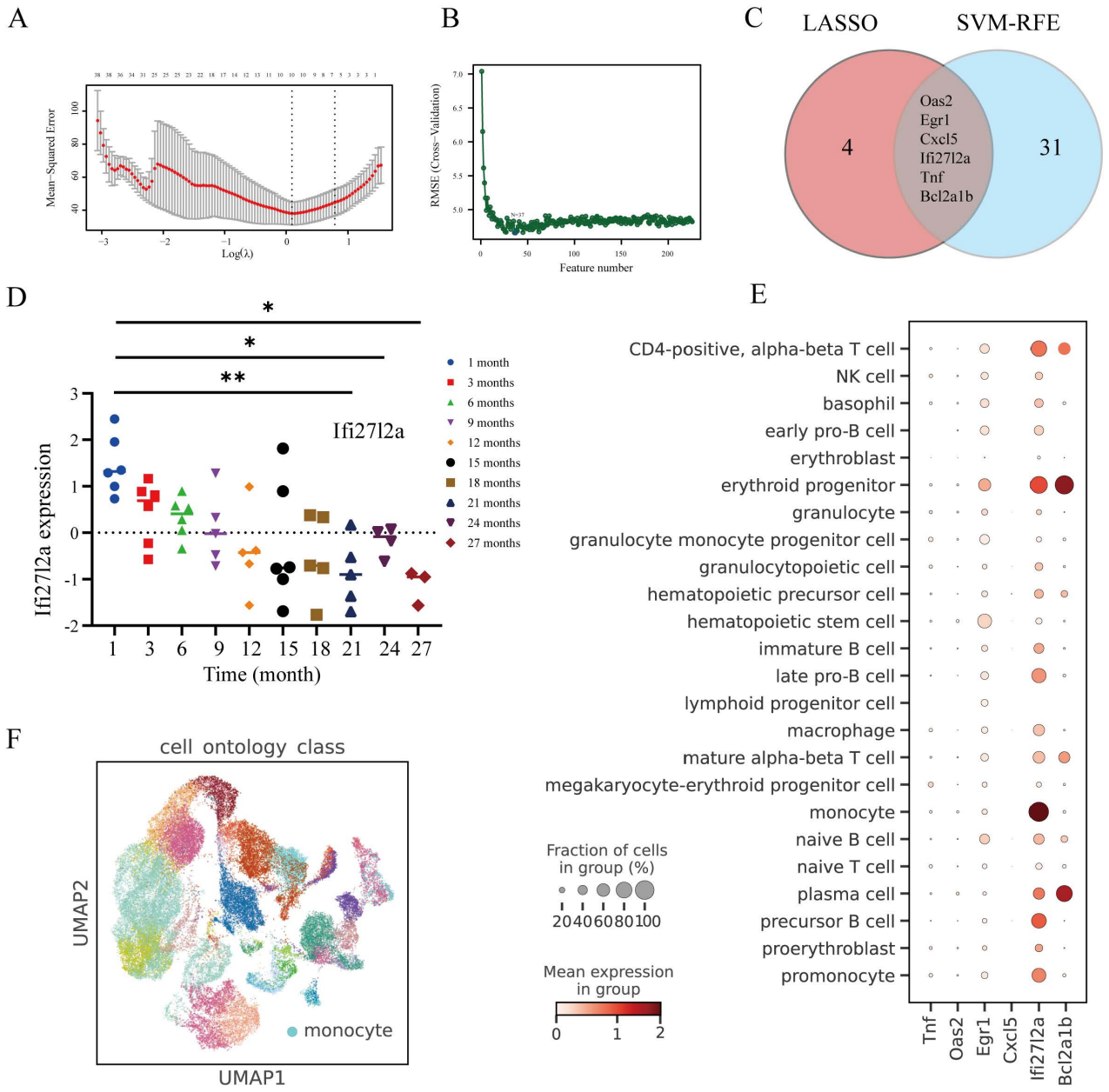

Fig. 2. Feature-selection-based prioritization and cellular distribution of candidate aging-associated genes in mouse bone marrow. (A) Least absolute shrinkage and selection operator (LASSO) regression analysis of age-associated DEGs. The plot shows the mean squared error across the logarithm of the penalty parameter λ. The upper x-axis indicates the number of retained features, and the vertical dashed line marks the optimal lambda value used for feature selection. (B) Support vector machine-recursive feature elimination (SVM-RFE)-based feature optimization. The plot shows cross-validation root mean squared error (RMSE) during recursive feature elimination and indicates the feature subset with the lowest RMSE under the optimized model. (C) Venn diagram showing the overlap between candidate genes identified by LASSO regression and SVM-RFE. LASSO retained 10 genes, SVM-RFE selected 37 genes, and six shared genes, including *Ifi27l2a*, *Oas2*, *Egr1*, *Cxcl5*, *Tnf*, and *Bcl2a1b*, were retained for further evaluation. (D) Expression pattern of *Ifi27l2a* across different age groups in the bulk RNA-seq dataset. (E) Dot plot showing the expression profiles of candidate genes across annotated bone marrow cell populations. Dot size indicates the percentage of cells expressing each gene, and color intensity represents the average expression level. (F) Uniform Manifold Approximation and Projection (UMAP) visualization of mouse bone marrow cells from the single-cell RNA-seq dataset, highlighting the monocyte-related compartment within the bone marrow cell landscape. Asterisks indicate statistical significance for the indicated comparisons: $p < 0.05$ for a single asterisk and $p < 0.01$ for double asterisks.

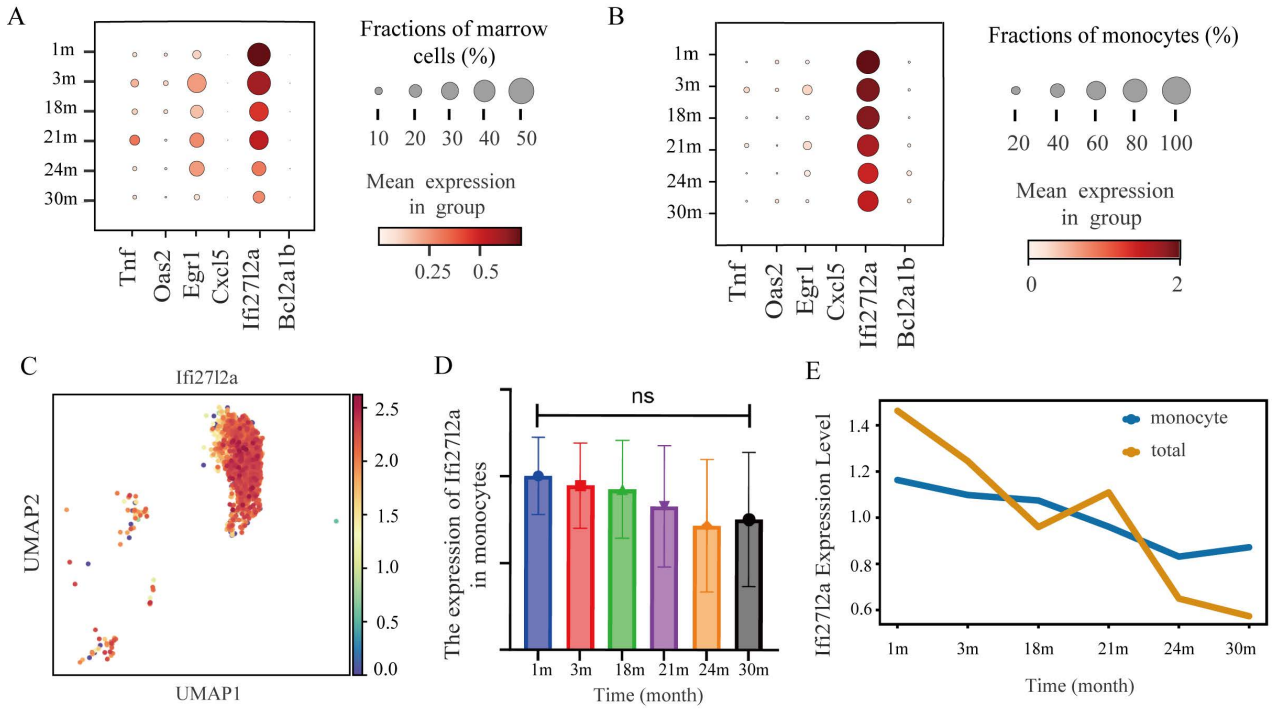

Fig. 3. Single-cell analysis of *Ifi27l2a* expression in mouse bone marrow during aging, with emphasis on the monocyte compartment. (A) Dot plot showing the age-associated expression profiles of candidate genes in total bone marrow cells. Dot size indicates the fraction of marrow cells expressing each gene, and color intensity represents the mean expression level in each age group. (B) Dot plot showing the expression profiles of candidate genes in bone marrow monocytes across age groups. Dot size indicates the fraction of monocytes expressing each gene, and color intensity represents the mean expression level in each age group. (C) UMAP visualization of *Ifi27l2a* expression in the annotated monocyte population from the single-cell RNA-seq dataset. Each dot represents a single cell, and color intensity indicates log-normalized *Ifi27l2a* expression. (D) Quantification of mean *Ifi27l2a* expression in bone marrow monocytes across age groups. No significant age-dependent difference was observed. (E) Comparison of age-associated *Ifi27l2a* expression trends between total bone marrow cells and the monocyte subset. ns indicates no statistically significant difference ($p \geq 0.05$).

TRAP-positive multinucleated morphology (Fig. 4B). This observation provided primary-cell-based morphological support for a possible association between *Ifi27l2a* knockdown and altered osteoclast-like changes.

The expression of selected inflammatory mediators was next assessed. RT-qPCR analysis showed that *Il6* and *Tnf* mRNA levels were significantly lower in SH3 cells than in SHB cells (Fig. 4D,E). Consistently, RNA-seq-derived normalized read counts showed a similar downward pattern for *Il6* and *Tnf* in the *Ifi27l2a* knockdown group (Fig. 4G,H). These results indicate that *Ifi27l2a* knockdown was accompanied by reduced expression of these inflammatory mediators in macrophage-lineage cells.

RNA-seq analysis was further performed to characterize broader transcriptional changes associated with *Ifi27l2a* knockdown. Hierarchical clustering showed clear separation between SHB and SH3 samples, indicating distinct transcriptomic profiles after knockdown (Fig. 4I). Differential expression analysis identified 174 differentially expressed genes, including 146 upregulated and 28 downregulated genes in SH3 cells compared with SHB cells (Fig. 4J). Together, these results confirm effective *Ifi27l2a* depletion and show that *Ifi27l2a* knockdown is accompanied by inflammatory gene changes, macrophage-lineage transcriptomic remodeling, and altered TRAP-positive osteoclast-like morphology.

3.5 Ifi27l2a *Knockdown is Associated With Inflammatory Pathway Remodeling and Osteoclast-Related Transcriptional Changes*

As shown in Fig. 5A, pathway enrichment analysis indicated that differentially expressed genes after *Ifi27l2a* knockdown were mainly associated with immune- and inflammation-related pathways, including “rheumatoid arthritis”, “TNF signaling pathway”, “Ras signaling pathway”, “JAK-STAT signaling pathway”, and “osteoclast differentiation”. These enriched pathways suggest that *Ifi27l2a* knockdown is accompanied by transcriptional remodeling of inflammatory and osteoclast-related signaling programs, rather than activation of a single linear pathway.

The heatmap presented in Fig. 5B showed distinct expression patterns of genes associated with “osteoclast differentiation” and “rheumatoid arthritis” between SH3 and

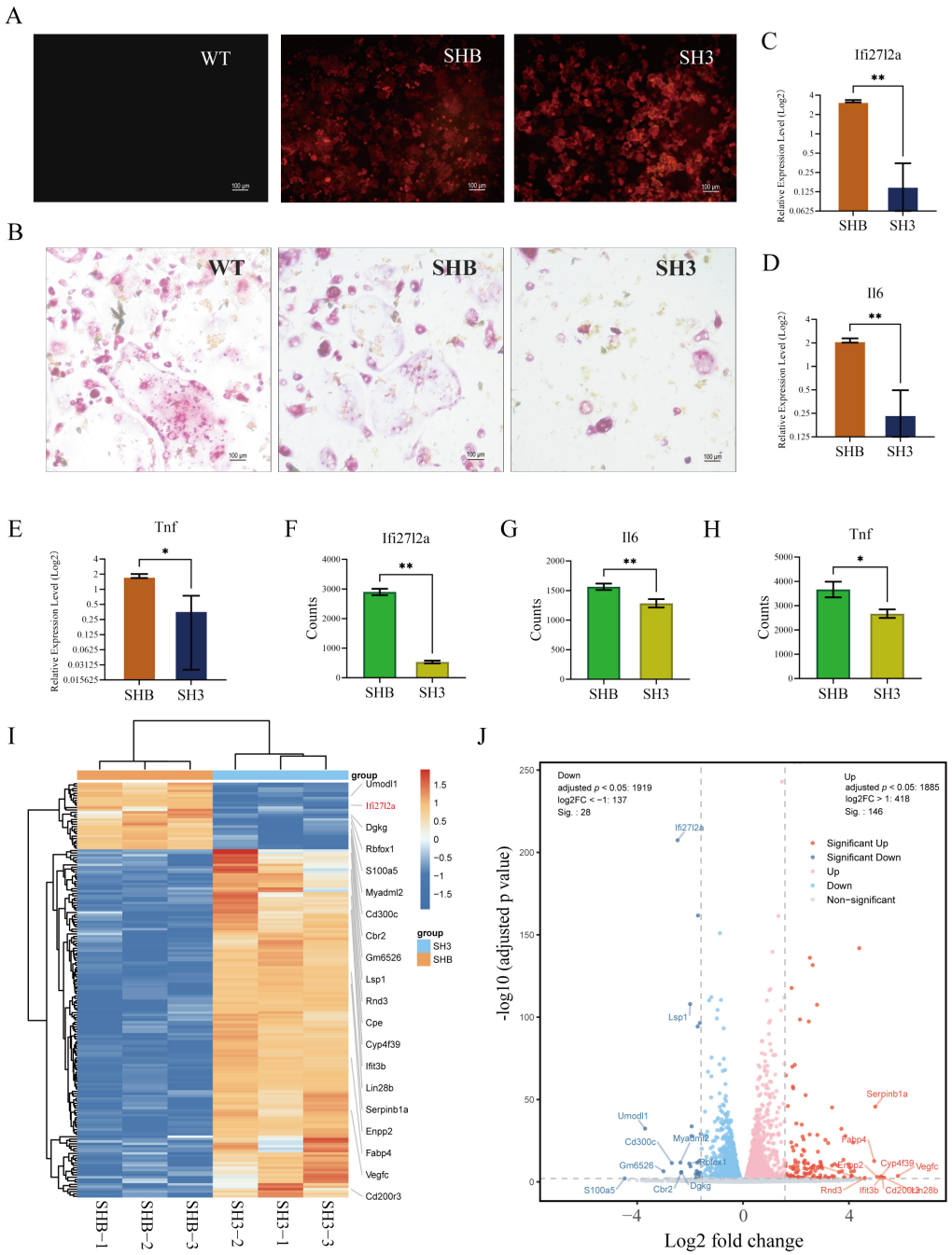

Fig. 4. *Ifi27l2a* knockdown is associated with inflammatory gene changes, transcriptomic remodeling, and osteoclast-like morphological alterations. (A) RFP fluorescence images of WT, SHB, and SH3 cells after lentiviral transduction. WT, untreated control cells; SHB, cells transduced with a non-targeting shRNA; SH3, cells transduced with an *Ifi27l2a*-targeting shRNA. Scale bars = 100 µm. (B) TRAP staining of primary bone marrow-derived macrophages (BMMs) after M-CSF/RANKL-induced osteoclastogenic stimulation in the WT, SHB, and SH3 groups, showing osteoclast-like morphological changes. Scale bars = 100 µm. (C) RT-qPCR validation of *Ifi27l2a* mRNA depletion in SH3 cells compared with SHB cells, normalized to Gapdh. (D,E) RT-qPCR analysis of *Il6* (D) and *Tnf* (E) mRNA expression in SHB and SH3 cells, normalized to Gapdh. (F–H) RNA-seq-derived normalized read counts of *Ifi27l2a* (F), *Il6* (G), and *Tnf* (H) in SHB and SH3 cells. (I) Hierarchical clustering heatmap of differentially expressed genes, showing distinct transcriptomic profiles between SHB and SH3 cells. (J) Volcano plot showing differentially expressed genes between SHB and SH3 cells. Red dots indicate significantly upregulated genes, blue dots indicate significantly downregulated genes, and grey dots indicate non-significant genes. A total of 174 differentially expressed genes were identified, including 146 upregulated and 28 downregulated genes in SH3 cells compared with SHB cells. For (C–H), $*p < 0.05$ and $**p < 0.01$.

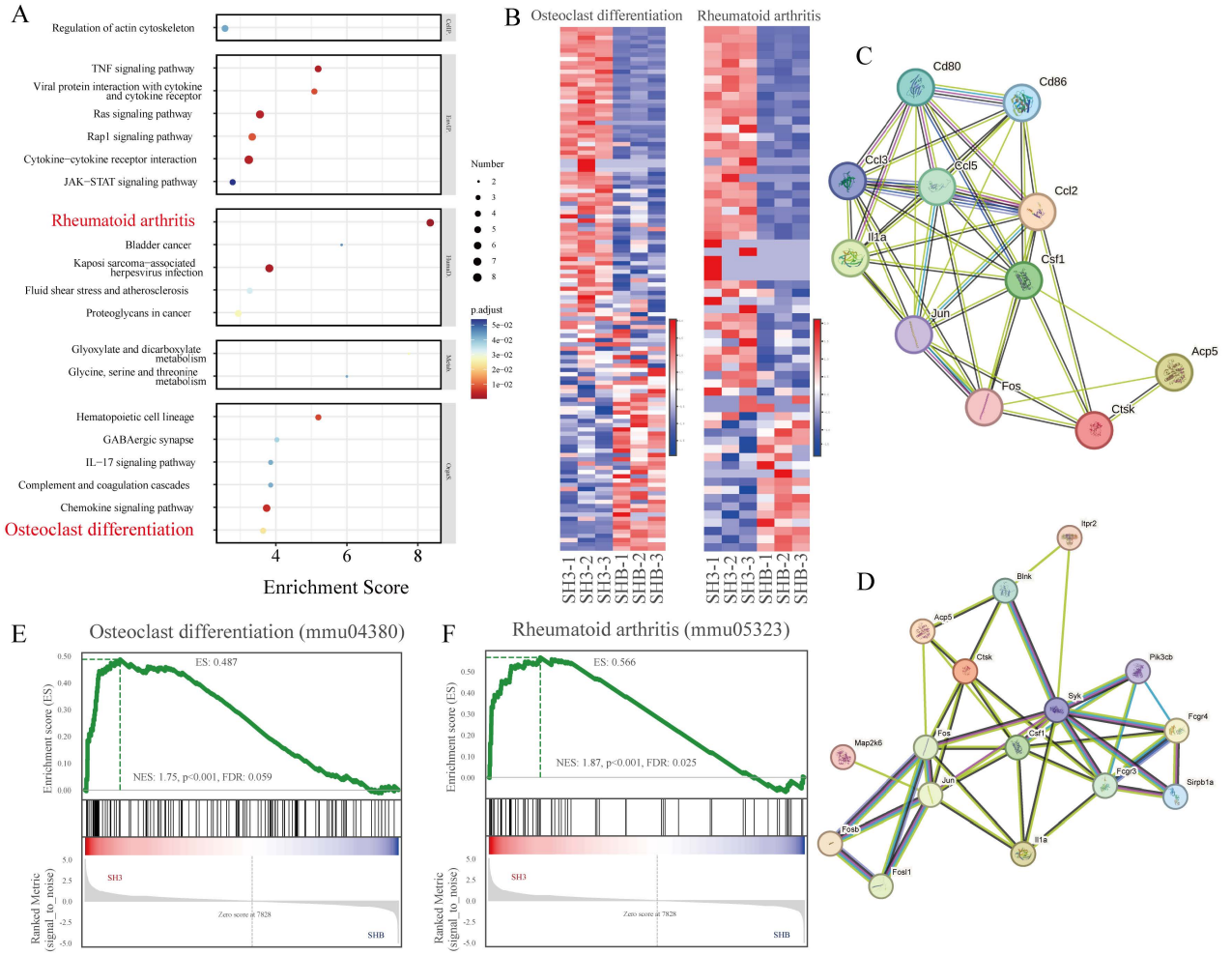

Fig. 5. Pathway enrichment and gene interaction analyses following *Ifi27l2a* knockdown. (A) Pathway enrichment analysis showing enriched pathways in knockdown cells, with highlighted pathways including "rheumatoid arthritis", "osteoclast differentiation", "TNF signaling pathway", "Ras signaling pathway", and "JAK-STAT signaling pathway" (size indicates gene count; color represents significance). (B) Heatmap displaying expression clusters of gene sets associated with "osteoclast differentiation" and "rheumatoid arthritis", showing distinct expression patterns between SH3 and SHB sample groups; upregulated genes in the SH3 group are indicated (red = high expression, blue = low expression). (C) Gene interaction network of the rheumatoid arthritis-associated cluster, including key genes: *Ctsk*, *Ccl2*, *Acp5*, *Il1a*, *Csf1*, *Ccl5*, *Cd80*, *Cd86*, *Ccl3*, *Jun*, and *Fos*. (D) Gene interaction network of the osteoclast differentiation-related cluster, including key genes: *Ctsk*, *Acp5*, *Il1a*, *Fosl1*, *Csf1*, *Fcgr3*, *Blnk*, *Sirpb1a*, *Syk*, *Pik3cb*, *Map2k6*, *Itpr2*, *Fosb*, *Fcgr4*, *Jun,* and *Fos*. (E) GSEA plot for the "osteoclast differentiation (mmu04380)" pathway, showing suggestive positive enrichment in SH3 cells compared with SHB cells (ES = 0.487, NES = 1.75, nominal $p < 0.001$, FDR = 0.059). (F) GSEA plot for the "rheumatoid arthritis (mmu05323)" pathway, showing significant positive enrichment in SH3 cells compared with SHB cells (ES = 0.566, NES = 1.87, nominal $p < 0.001$, FDR = 0.025).

SHB cells. Gene interaction network analysis further identified several inflammation- and osteoclast-related genes within these pathway clusters, including *Ctsk*, *Acp5*, *Ccl2*, *Il1a*, *Csf1*, *Jun*, and *Fos* (Fig. 5C,D). These results indicate that the transcriptional changes induced by *Ifi27l2a* knockdown involve interconnected inflammatory and osteoclast-related gene networks.

GSEA showed significant positive enrichment of the "rheumatoid arthritis" pathway in SH3 cells compared with SHB cells (NES = 1.87, nominal $p < 0.001$, FDR = 0.025; Fig. 5F). The "osteoclast differentiation" pathway also showed a suggestive positive enrichment pattern (NES = 1.75, nominal $p < 0.001$, FDR = 0.059; Fig. 5E), although the FDR value was borderline and did not meet the conventional threshold for strong significance. Together, these results suggest that *Ifi27l2a* knockdown is associated with inflammatory pathway remodeling and may be linked to osteoclast-related transcriptional changes in macrophage-lineage cells.

4. Discussion

This study identified *Ifi27l2a* as an aging-associated candidate gene in mouse bone marrow by integrating bulk RNA-seq analysis, LASSO and SVM-RFE feature selection, single-cell RNA-seq analysis, and cellular validation. In the bulk RNA-seq dataset, aged bone marrow exhibited a distinct transcriptional profile compared with young bone marrow, with differentially expressed genes mainly enriched in immune- and virus-response-related biological processes. This pattern is consistent with the concept of inflammaging, in which chronic low-grade immune dysregulation reshapes tissue microenvironments and contributes to age-related functional decline [20]. In the skeletal system, inflammaging has been linked to age-related bone diseases by disturbing the balance among osteogenesis, osteoclastogenesis, adipogenesis, and chondrogenesis [21]. Inflammation and aging are also closely associated with impaired bone remodeling and reduced regenerative capacity [22]. Given that bone marrow is both a hematopoietic and immune-active tissue, age-related remodeling of the bone marrow immune microenvironment may influence skeletal homeostasis, particularly through changes in monocyte/macrophage-lineage cells [23,24].

LASSO and SVM-RFE analyses narrowed the age-associated DEGs to six overlapping candidate genes: *Ifi27l2a*, *Oas2*, *Egr1*, *Cxcl5*, *Tnf*, and *Bcl2a1b*. Among them, *Ifi27l2a* showed a consistent decrease in whole bone marrow and was selected for further analysis. Single-cell RNA-seq analysis placed *Ifi27l2a* mainly within the monocyte-related compartment, while its expression within monocytes remained relatively stable across age groups. Therefore, the reduced *Ifi27l2a* expression observed in whole bone marrow may reflect both transcriptional changes and age-related shifts in bone marrow cellular composition. This interpretation is consistent with single-cell evidence showing that osteoporosis-related bone loss may involve an imbalance in monocyte subsets rather than uniform transcriptional changes within all monocytes [25]. In addition, single-cell integration has been increasingly used to assign bone-related candidate genes to specific cellular compartments, highlighting the importance of cell-type resolution when interpreting bulk bone marrow transcriptomic changes [13]. Since monocyte/macrophage-lineage cells include osteoclast precursors, alterations in this compartment may influence osteoclast-lineage remodeling during aging [26,27,28].

Ifi27l2a belongs to the ISG12/IFI27-related interferon-stimulated gene family. Previous studies have described the ISG12 family composition in humans and mice and linked ISG12-related genes to interferon-responsive transcriptional programs [29,30]. ISG12 has also been reported to modulate innate immune responses and inflammatory cytokine production in macrophage-related inflammatory models [31]. More recent evidence further supports the involvement of *Ifi27l2a* in inflammatory and myeloid-lineage contexts. In the central nervous system, *Ifi27l2a* was identified as a regulator of microglial inflammation during aging and stroke [32]. More directly related to skeletal remodeling, a recent single-cell study reported that *Ifi27l2a* was upregulated in bone marrow monocytes in glucocorticoid-induced osteoporosis and contributed to enhanced osteoclast differentiation and bone loss [33]. These findings support the biological relevance of *Ifi27l2a* in monocyte/macrophage-lineage inflammatory regulation and osteoclast-related remodeling. However, the direction of *Ifi27l2a* alteration appears to be context-dependent. In contrast to the glucocorticoid-induced osteoporosis model, the present aging-related bone marrow analysis showed reduced *Ifi27l2a* expression at the bulk level and a more complex cellular response after *Ifi27l2a* knockdown. Thus, *Ifi27l2a* should be interpreted as a context-sensitive gene associated with macrophage-lineage and osteoclast-related states, rather than as a unidirectional driver of osteoclastogenesis.

In the cellular validation experiments, *Ifi27l2a* knockdown in RAW264.7 cells decreased Il6 and Tnf expression at both the RT-qPCR and RNA-seq levels, supporting a relationship between *Ifi27l2a* and inflammatory mediator expression in macrophage-lineage cells. Transcriptomic analysis confirmed efficient knockdown in SH3 cells compared with the non-targeting shRNA control group SHB, with *Ifi27l2a* showing a fold change of 0.18 and a $\log_2$FoldChange of -2.47. Beyond *Ifi27l2a* repression, RNA-seq analysis identified 174 DEGs between SH3 and SHB cells, including 146 upregulated and 28 downregulated genes. Several osteoclast-associated or macrophage-remodeling-related transcripts, including *Acp5*, *Ctsk*, *Atp6v0d2*, *Itgax*, *Timp1*, *Mcoln2*, *Lims2*, and *Clstn3*, were upregulated in SH3 cells. This suggests that *Ifi27l2a* knockdown reshaped macrophage-lineage gene-expression programs involving osteoclast-related features. However, these transcriptomic changes should not be directly equated with enhanced osteoclast maturation or bone-resorptive function. *Acp5* and *Ctsk* are commonly associated with RANKL-induced osteoclast activation, whereas osteoclast formation requires coordinated macrophage-lineage differentiation, precursor fusion, multinucleation, cytoskeletal organization, and acquisition of bone-resorptive function [26,34,35]. Recent single-cell multi-omics evidence also suggests that osteoclastogenesis during aging involves coordinated transcriptional regulation rather than a single linear pathway [36]. In addition, *Ccl2* is involved in monocyte recruitment and skeletal inflammatory remodeling [37], while Fos and Jun are central components of AP-1-related signaling in bone development and inflammatory bone disease [38]. Therefore, the increased expression of osteoclast-associated transcripts in SH3 cells may reflect a shift in macrophage-lineage transcriptional state rather than direct evidence of fully enhanced osteoclast formation.

The pathway enrichment results further supported this cautious interpretation. The rheumatoid arthritis pathway showed significant positive enrichment after *Ifi27l2a* knockdown, which is biologically relevant because rheumatoid arthritis is characterized by immune-mediated inflammation and bone erosion [39]. Suppression of inflammatory pathways in rheumatoid arthritis can also reduce local and systemic bone loss, supporting the close relationship between immune activation and bone remodeling [40]. In contrast, the osteoclast differentiation pathway showed only suggestive positive enrichment, with a borderline FDR value. Thus, the enrichment results indicate osteoclast-related transcriptional remodeling but do not establish strong activation of the osteoclast differentiation pathway.

The primary BMM experiment further provided functional support at the cellular level. RAW264.7 cells were used for transcriptomic and inflammatory gene-expression analyses, whereas primary BMMs were used for osteoclast differentiation validation. Primary BMMs are more physiologically relevant for evaluating osteoclast-like differentiation under M-CSF/RANKL stimulation, as osteoclasts originate from monocyte/macrophage-lineage precursors and acquire bone-resorptive activity through coordinated differentiation and fusion [26,35]. After induction, WT and SHB BMMs showed TRAP-positive osteoclast-like cell formation, whereas SH3 cells displayed a less prominent TRAP-positive multinucleated osteoclast-like morphology. This supports an association between reduced *Ifi27l2a* expression and altered osteoclast-like differentiation in primary macrophage-lineage cells.

The apparent discrepancy between osteoclast-associated transcript upregulation in RAW264.7 cells and less prominent osteoclast-like differentiation in primary BMMs may reflect the complexity of the macrophage-to-osteoclast transition. Osteoclastogenesis requires not only the expression of individual osteoclast-associated genes but also coordinated precursor commitment, cell fusion, multinucleation, cytoskeletal organization, and functional maturation [26,35]. Therefore, partial transcriptional activation of osteoclast-related genes may occur without complete osteoclast maturation. In addition, the transcriptomic profile suggested possible changes in Wnt-associated regulatory events. Since canonical Wnt/β-catenin signaling has been reported to negatively regulate osteoclast differentiation in osteoclast-lineage cells, these changes raise the possibility that Wnt-related regulation may contribute to the uncoupling between osteoclast-associated gene expression and functional osteoclast-like differentiation [41,42]. However, because the present study did not directly measure β-catenin activation, nuclear β-catenin accumulation, Wnt reporter activity, or rescue effects after Wnt pathway inhibition, this interpretation remains hypothetical and requires further validation. Previous proteomic comparison has also shown that osteoclasts derived from RAW264.7 cells and primary BMMs differ substantially in their cellular characteristics, supporting the need to interpret these two systems separately [43].

In summary, *Ifi27l2a* is associated with bone marrow aging, monocyte-related immune remodeling, and osteoclast-lineage regulation. The current data do not support a simple model in which *Ifi27l2a* reduction directly drives bone degeneration or uniformly enhances osteoclastogenesis. Instead, *Ifi27l2a* knockdown appears to reshape macrophage-lineage transcriptional states involving inflammatory mediator expression, chemokine signaling, osteoclast-related gene programs, and possible Wnt-associated regulatory changes. Together with recent evidence from glucocorticoid-induced osteoporosis and aging-related inflammatory models, our findings suggest that *Ifi27l2a* may function in a context-dependent manner within monocyte/macrophage-lineage remodeling. Further *in vivo* studies and pathway-level validation are needed to determine whether this regulatory pattern contributes directly to age-related bone loss.

5. Limitations

The present study used publicly available bulk RNA-seq and single-cell RNA-seq datasets to investigate aging-related transcriptional changes in bone marrow. Although these analyses supported the identification of *Ifi27l2a* as a bone marrow aging-associated candidate gene, they did not establish causality. Because the bulk RNA-seq data were derived from whole bone marrow, the reduced *Ifi27l2a* expression may reflect both transcriptional changes in specific cell populations and age-related shifts in cellular composition. In addition, the single-cell analysis did not include refined monocyte subpopulation annotation, trajectory inference, or cell–cell communication analysis, which limited the interpretation of bone marrow inflammaging-related cellular dynamics.

Experimental validation was performed mainly in macrophage-lineage cell models. RAW264.7 cells are useful for examining inflammatory and osteoclast-related responses but cannot fully represent primary osteoclast precursors. The added primary BMM-based TRAP staining assay provided morphological support in a primary macrophage-lineage system; however, further quantitative osteoclast assays, bone resorption assays, rescue experiments, and *in vivo* bone phenotype validation are still required to determine whether *Ifi27l2a* directly regulates osteoclast differentiation or age-related bone loss. Future studies using aged animal models combined with micro-CT, bone histology, tissue-level TRAP staining, and expanded single-cell analyses will help clarify the role of *Ifi27l2a* in age-related bone remodeling.

6. Conclusion

This study identified *Ifi27l2a* as a bone marrow aging-associated candidate gene through integrated bulk RNA-

seq and single-cell RNA-seq analyses. *Ifi27l2a* expression was reduced in aged whole bone marrow and showed a monocyte-enriched distribution at the single-cell level, suggesting its potential relevance to immune remodeling during bone marrow aging. In macrophage-lineage cells, *Ifi27l2a* knockdown altered the expression of inflammatory mediators and reshaped the transcriptomic profile, with changes involving inflammatory programs and suggestive osteoclast-related transcriptional remodeling. The primary BMM-based TRAP staining assay further provided morphological support for a possible association between *Ifi27l2a* reduction and osteoclast-like changes under M-CSF/RANKL stimulation. Overall, these findings suggest that *Ifi27l2a* may be associated with inflammatory and osteoclast-lineage remodeling in the aging bone marrow microenvironment, providing a potential molecular clue for further investigation of age-related bone remodeling.

Abbreviations

DEGs, Differentially Expressed Genes; GO, Gene Ontology; KEGG, Kyoto Encyclopedia of Genes and Genomes; GSEA, Gene Set Enrichment Analysis; LASSO, Least Absolute Shrinkage and Selection Operator; SVM-RFE, Support Vector Machine-Recursive Feature Elimination; FPKM, Fragments Per Kilobase Million; RT-qPCR, Reverse Transcription-Quantitative Polymerase Chain Reaction; TNF, Tumor Necrosis Factor; IL-6, Interleukin-6; RANKL, Receptor Activator of Nuclear Factor-κB Ligand; M-CSF, Macrophage Colony-Stimulating Factor; scRNA-seq, Single-Cell RNA Sequencing; GEO, Gene Expression Omnibus; NES, Normalized Enrichment Score; FDR, False Discovery Rate.

Availability of Data and Materials

The public datasets analyzed in this study are available in the GEO database under accession numbers GSE132040 and GSE132042. The RNA-seq data generated in this study and other supporting data are available from the corresponding authors upon reasonable request.

Author Contributions

LW and LJ conceived and designed the study, served as project leaders, and supervised the overall research process. YL performed cell culture and maintenance, total RNA extraction, and concentration/purity detection; led RT-qPCR experiments, including assay optimization, data collection and analysis; generated core experimental data; and drafted the initial version of the manuscript. JM assisted in RNA extraction and contributed to partial data analysis. WZ and YX conducted RNA concentration and purity assessment using a NanoDrop 2000 spectrophotometer. All authors contributed to editorial changes in the manuscript. All authors read and approved the final manuscript. All authors have participated sufficiently in the work and agreed to be accountable for all aspects of the work.

Ethics Approval and Consent to Participate

The animal study protocol for the isolation of primary bone marrow-derived macrophages from C57BL/6 mice was approved by the Committee of the Northwest Institute of Plateau Biology, Chinese Academy of Sciences (License No. NWIPB2025–46). All animal-related procedures were conducted in accordance with the Chinese national standard Laboratory Animal—Guideline for Ethical Review of Animal Welfare (GB/T 35892-2018) and the institutional guidelines for the care and use of laboratory animals of the Northwest Institute of Plateau Biology, Chinese Academy of Sciences. The study was reported in accordance with the ARRIVE guidelines.

Acknowledgment

Not applicable.

Funding

This research was funded by the Key Research, Development and Transformation Program of Qinghai Province (2024-SF-127).

Conflicts of Interest

The authors declare no conflicts of interest.

Supplementary Material

Supplementary material associated with this article can be found, in the online version, at https://doi.org/10.31083/FBL50499.

References

[1] Mi B, Xiong Y, Knoedler S, Alfertshofer M, Panayi AC, Wang H, et al. Ageing-related bone and immunity changes: insights into the complex interplay between the skeleton and the immune system. Bone Research. 2024; 12: 42. https://doi.org/10.1038/s41413-024-00346-4

[2] Wang J, Xin Y, Dong Z, Li S, Yang G. The interplay between the immune microenvironment and bone aging: From molecular mechanisms to therapeutic interventions. Experimental Gerontology. 2025; 212: 112974. https://doi.org/10.1016/j.exger.2025.112974

[3] Hofmann J, Kokkaliaris KD. Bone marrow niches for hematopoietic stem cells: life span dynamics and adaptation to acute stress. Blood. 2024; 144: 21–34. https://doi.org/10.1182/blood.2023023788

[4] Gao X, Zhang J, Tamplin OJ. The aging hematopoietic stem cell niche: a mini review. Frontiers in Hematology. 2025; 4: 1525132. https://doi.org/10.3389/frhem.2025.1525132

[5] Hou J, Chen KX, He C, Li XX, Huang M, Jiang YZ, et al. Aged bone marrow macrophages drive systemic aging and age-related dysfunction via extracellular vesicle-mediated induction of paracrine senescence. Nature Aging. 2024; 4: 1562–1581. https://doi.org/10.1038/s43587-024-00694-0

[6] Li Y, Chen H, Zhou S. Macrophages and Tissue Homeostasis: From Physiological Functions to Disease Onset. Frontiers in Bioscience (Landmark Edition). 2025; 30: 42706. https://doi.org/10.31083/fbl42706
[7] Cai L, Lv Y, Yan Q, Guo W. Cytokines: The links between bone and the immune system. Injury. 2024; 55: 111203. https://doi.org/10.1016/j.injury.2023.111203
[8] Qi Z, Luo J, Xiao Z, Yang D. Functional roles of immune cells in osteoporosis. Frontiers in Immunology. 2025; 16: 1698283. https://doi.org/10.3389/fimmu.2025.1698283
[9] Kirkham-Wilson F, Dennison E. Osteoporosis and Rheumatoid Arthritis: A Review of Current Understanding and Practice. British Journal of Hospital Medicine (London, England : 2005). 2024; 85: 1–11. https://doi.org/10.12968/hmed.2024.0341
[10] Oelzner P, Mueller PH, Hoffmann T, Schwabe A, Lehmann G, Eidner T, et al. Significant decrease of osteoporosis and osteoporotic fractures in rheumatoid arthritis within a period of 24 years: experiences of a single centre. RMD Open. 2024; 10: e004564. https://doi.org/10.1136/rmdopen-2024-004564
[11] Tabula Muris Consortium, Overall coordination, Logistical coordination, Organ collection and processing, Library preparation and sequencing, Computational data analysis, et al. Single-cell transcriptomics of 20 mouse organs creates a Tabula Muris. Nature. 2018; 562: 367–372. https://doi.org/10.1038/s41586-018-0590-4
[12] Tabula Muris Consortium. A single-cell transcriptomic atlas characterizes ageing tissues in the mouse. Nature. 2020; 583: 590–595. https://doi.org/10.1038/s41586-020-2496-1
[13] Doolittle ML, Khosla S, Saul D. Single-Cell Integration of BMD GWAS Results Prioritize Candidate Genes Influencing Age-Related Bone Loss. JBMR Plus. 2023; 7: e10795. https://doi.org/10.1002/jbm4.10795
[14] Love MI, Huber W, Anders S. Moderated estimation of fold change and dispersion for RNA-seq data with DESeq2. Genome Biology. 2014; 15: 550. https://doi.org/10.1186/s13059-014-0550-8
[15] Wu T, Hu E, Xu S, Chen M, Guo P, Dai Z, et al. clusterProfiler 4.0: A universal enrichment tool for interpreting omics data. Innovation (Cambridge (Mass.)). 2021; 2: 100141. https://doi.org/10.1016/j.xinn.2021.100141
[16] Friedman J, Hastie T, Tibshirani R. Regularization Paths for Generalized Linear Models via Coordinate Descent. Journal of Statistical Software. 2010; 33: 1–22.
[17] Kuhn M. Building Predictive Models in R Using the caret Package. Journal of Statistical Software. 2008; 28: 1–26. https://doi.org/10.18637/jss.v028.i05
[18] Wolf FA, Angerer P, Theis FJ. SCANPY: large-scale single-cell gene expression data analysis. Genome Biology. 2018; 19: 15. https://doi.org/10.1186/s13059-017-1382-0
[19] Polański K, Young MD, Miao Z, Meyer KB, Teichmann SA, Park JE. BBKNN: fast batch alignment of single cell transcriptomes. Bioinformatics (Oxford, England). 2020; 36: 964–965. https://doi.org/10.1093/bioinformatics/btz625
[20] Li X, Li C, Zhang W, Wang Y, Qian P, Huang H. Inflammation and aging: signaling pathways and intervention therapies. Signal Transduction and Targeted Therapy. 2023; 8: 239. https://doi.org/10.1038/s41392-023-01502-8
[21] Bi J, Zhang C, Lu C, Mo C, Zeng J, Yao M, et al. Age-related bone diseases: Role of inflammaging. Journal of Autoimmunity. 2024; 143: 103169. https://doi.org/10.1016/j.jaut.2024.103169
[22] Kushioka J, Chow SKH, Toya M, Tsubosaka M, Shen H, Gao Q, et al. Bone regeneration in inflammation with aging and cell-based immunomodulatory therapy. Inflammation and Regeneration. 2023; 43: 29. https://doi.org/10.1186/s41232-023-00279-1
[23] Lambert C, Wu Y, Aanei C. Bone Marrow Immunity and Myelodysplasia. Frontiers in Oncology. 2016; 6: 172. https://doi.org/10.3389/fonc.2016.00172
[24] Pappert M, Khosla S, Doolittle M. Influences of Aged Bone Marrow Macrophages on Skeletal Health and Senescence. Current Osteoporosis Reports. 2023; 21: 771–778. https://doi.org/10.1007/s11914-023-00820-8
[25] Tao L, Jiang W, Li H, Wang X, Tian Z, Yang K, et al. Single-cell RNA sequencing reveals that an imbalance in monocyte subsets rather than changes in gene expression patterns is a feature of postmenopausal osteoporosis. Journal of Bone and Mineral Research : the Official Journal of the American Society for Bone and Mineral Research. 2024; 39: 980–993. https://doi.org/10.1093/jbmr/zjae065
[26] Elson A, Anuj A, Barnea-Zohar M, Reuven N. The origins and formation of bone-resorbing osteoclasts. Bone. 2022; 164: 116538. https://doi.org/10.1016/j.bone.2022.116538
[27] Thiyagarajan R, Zhang L, Glover OD, Kwack KH, Ahmed S, Murray E, et al. Age-related increase of CD38 directs osteoclastogenic potential of monocytic myeloid-derived suppressor cells through mitochondrial dysfunction in male mice. Aging Cell. 2024; 23: e14298. https://doi.org/10.1111/acel.14298
[28] Kaneko K, Tsai J, Meñez D, Oh B, Suh AJ, Bae S, et al. Cellular signatures in human blood track bone mineral density in postmenopausal women. JCI Insight. 2024; 9: e178977. https://doi.org/10.1172/jci.insight.178977
[29] Jin W, Jin W, Pan D. Ifi27 is indispensable for mitochondrial function and browning in adipocytes. Biochemical and Biophysical Research Communications. 2018; 501: 273–279. https://doi.org/10.1016/j.bbrc.2018.04.234
[30] Certa U, Seiler M, Padovan E, Spagnoli GC. High density oligonucleotide array analysis of interferon- alpha2a sensitivity and transcriptional response in melanoma cells. British Journal of Cancer. 2001; 85: 107–114. https://doi.org/10.1054/bjoc.2001.1865
[31] Uhrin P, Perkmann T, Binder B, Schabbauer G. ISG12 is a critical modulator of innate immune responses in murine models of sepsis. Immunobiology. 2013; 218: 1207–1216. https://doi.org/10.1016/j.imbio.2013.04.009
[32] Kim GS, Harmon E, Gutierrez MC, Kim S, Vance L, Burrous H, et al. Single-cell analysis identifies Ifi27l2a as a gene regulator of microglial inflammation in the context of aging and stroke in mice. Nature Communications. 2025; 16: 1639. https://doi.org/10.1038/s41467-025-56847-1
[33] Wang Z, Huang C, Liu S, Xiao P, Lu Z, Xu Y, et al. Up-regulation of Ifi27l2a expression in bone marrow monocytes contributes to glucocorticoid-induced bone loss. Communications Biology. 2025; 8: 1590. https://doi.org/10.1038/s42003-025-08985-x
[34] Ayyasamy R, Fan S, Czernik P, Lecka-Czernik B, Chattopadhyay S, Chakravarti R. 14-3-3ζ suppresses RANKL signaling by destabilizing TRAF6. The Journal of Biological Chemistry. 2024; 300: 107487. https://doi.org/10.1016/j.jbc.2024.107487
[35] Krishnacoumar B, Stenzel M, Garibagaoglu H, Omata Y, Sworn RL, Hofmann T, et al. Caspase-8 promotes scramblase-mediated phosphatidylserine exposure and fusion of osteoclast precursors. Bone Research. 2024; 12: 40. https://doi.org/10.1038/s41413-024-00338-4
[36] Li H, Xu WX, Tan JC, Hong YM, He J, Zhao BP, et al. Single-cell multi-omics identify novel regulators required for osteoclastogenesis during aging. iscience. 2024; 27: 110734. https://doi.org/10.1016/j.isci.2024.110734
[37] Zhu S, Liu M, Bennett S, Wang Z, Pfleger KDG, Xu J. The molecular structure and role of CCL2 (MCP-1) and C-C chemokine receptor CCR2 in skeletal biology and diseases. Journal of Cellular Physiology. 2021; 236: 7211–7222. https://doi.org/10.1002/jcp.30375
[38] Wagner EF. Bone development and inflammatory disease is reg-

ulated by AP-1 (Fos/Jun). Annals of the Rheumatic Diseases. 2010; 69 Suppl 1: i86–88. https://doi.org/10.1136/ard.2009.119396

[39] Smolen JS, Aletaha D, Barton A, Burmester GR, Emery P, Firestein GS, et al. Rheumatoid arthritis. Nature Reviews. Disease Primers. 2018; 4: 18001. https://doi.org/10.1038/nrdp.2018.1

[40] Zerbini CAF, Clark P, Mendez-Sanchez L, Pereira RMR, Messina OD, Uña CR, et al. Biologic therapies and bone loss in rheumatoid arthritis. Osteoporosis International : a Journal Established as Result of Cooperation between the European Foundation for Osteoporosis and the National Osteoporosis Foundation of the USA. 2017; 28: 429–446. https://doi.org/10.1007/s00198-016-3769-2

[41] Albers J, Keller J, Baranowsky A, Beil FT, Catala-Lehnen P, Schulze J, et al. Canonical Wnt signaling inhibits osteoclastogenesis independent of osteoprotegerin. The Journal of Cell Biology. 2013; 200: 537–549. https://doi.org/10.1083/jcb.201207142

[42] Weivoda MM, Ruan M, Hachfeld CM, Pederson L, Howe A, Davey RA, et al. Wnt Signaling Inhibits Osteoclast Differentiation by Activating Canonical and Noncanonical cAMP/PKA Pathways. Journal of Bone and Mineral Research : the Official Journal of the American Society for Bone and Mineral Research. 2016; 31: 65–75. https://doi.org/10.1002/jbmr.2599

[43] Ng AY, Tu C, Shen S, Xu D, Oursler MJ, Qu J, et al. Comparative Characterization of Osteoclasts Derived From Murine Bone Marrow Macrophages and RAW 264.7 Cells Using Quantitative Proteomics. JBMR Plus. 2018; 2: 328–340. https://doi.org/10.1002/jbm4.10058